Journal of Colloid and Interface Science **228,** 14–17 (2000)
doi:10.1006/jcis.2000.6923, available online at http://www.idealibrary.com on IDEAL®

# Latex Particle Size Distribution by Dynamic Light Scattering: Computer Evaluation of Two Alternative Calculation Paths

Luis M. Gugliotta, Jorge R. Vega, and Gregorio R. Meira[1]

*INTEC, Universidad Nacional del Litoral–CONICET, Güemes 3450, 3000 Santa Fe, Argentina*

Received June 8, 1999; accepted April 24, 2000

**Two calculation paths for estimating the particle size distribution (PSD) of a polymer latex from single-angle dynamic light scattering (DLS) measurements are evaluated on the basis of a numerical example. In the more common "double-step method," two calculation steps are applied, with the intermediate estimation of the particle light intensity distribution (PLID). In the "single-step method," the calculation is performed in one operation. From the specification of several PSDs, a mathematical model is used to produce the synthetic measurements. An iterative procedure was applied for determining the diameter range and the number of PSD points. The inversion operations were carried out using a regularization technique. For narrow distributions with diameters in the range 100–1000 nm, the PSD and the PLID are similar in shape, and both calculation paths produce similar results. For broad PSDs in the range 100–1000 nm, and for arbitrary PSDs in the range 10–100 nm (i.e., in the Rayleigh region), the single-step method proved preferable.** 

*Key Words:* **DLS; PSD; polymer latex; inverse problem.**

## INTRODUCTION

Optical methods, such as dynamic light scattering (DLS), static light scattering, and turbidimetry, are fast and reliable for evaluating average particle diameters, but they exhibit serious limitations for estimating the particle size distribution (PSD) (1–5).

In a DLS experiment, a dilute latex sample is irradiated with a monochromatic laser, and the temporal fluctuations of the scattered light due to the (Brownian) particle motion are determined. The raw DLS measurement is a discrete autocorrelation function of the scattered light intensity, $G^{(2)}(\tau_j)$, where $\tau_j$ represents the time delay. From such measurement, reproducible average particle diameters can be easily estimated through for example the cumulants method (6). The average diameter estimate (indicated here with $\hat{D}_{\text{cum}}$) cannot be associated to a specific PSD mean, but it is in general close to the so-called $D_{6,5}$ average, defined as $D_{6,5} = \sum f(D_i) D_i^6 / \sum f(D_i) D_i^5$, where $f(D_i)$ is the discrete number-particle diameter distribution. For distributions inside the Rayleigh region (i.e., with diameters smaller than 100 nm), $D_{\text{cum}}$ tends to $D_{6,5}$.

To estimate the PSD from a DLS measurement, Mie's theory is required (7), the particle refractive index must be known, and an (ill-posed) inversion problem must be solved. Several algorithms have been developed for solving the inversion problem: nonnegative least squares, the histogram method, singular value analysis, the subdistribution method, the maximum entropy technique, and the CONTIN program (8–10). DLS estimates are improved by taking measurements at several angles, but unfortunately such an advantage is lost for distributions inside the Rayleigh region (11, 12). A DLS measurement is affected by errors in the temperature, the medium viscosity, and the refractive indexes of the medium and particles. In this work, none of such errors will be considered, and furthermore, spherical and nonagglomerated latex particles will be assumed.

In what follows, two alternative paths for recuperating the PSD from single-angle DLS measurements are theoretically evaluated.

## THEORY

Define the PSD $f(D_i)$ with $n$ points evenly distributed along the diameter range $[D_{\min}, D_{\max}]$. The particle light intensity distribution (PLID), indicated by $h(D_i)$, is related to $f(D_i)$ through

$$h(D_i) = C_I(D_i) f(D_i), \quad (i = 1, \ldots, n), \qquad [1]$$

where the function $C_I(D_i)$ is obtained through Mie's theory (7) and represents the intensity fraction of light scattered by a particle of diameter $D_i$. The (first-order and normalized) autocorrelation of the electric field $g^{(1)}(\tau_j)$ is related to $h(D_i)$ through

$$g^{(1)}(\tau_j) = \Delta D \sum_{i=1}^{n} e^{-\frac{\Gamma_0 \tau_j}{D_i}} h(D_i), \quad (j = 1, \ldots, m), \qquad [2a]$$

with

$$\Gamma_0 = \frac{16\pi}{3} \left( \frac{n_{\text{m}}(\lambda)}{\lambda} \right)^2 \frac{kT}{\eta} \sin^2(\theta/2), \qquad [2b]$$

[1] To whom correspondence should be addressed. Fax: 54-342-455-0944. E-mail: gmeira@arcride.edu.ar.

0021-9797/00 $35.00

where $n_m(\lambda)$ is the (real) refractive index of the (nonabsorbing) medium, $k$ is Boltzmann's constant, $T$ is the absolute temperature, $\eta$ is the medium viscosity, and $\theta$ is the detection angle.

The noise-free "measurement" $G^{(2)}(\tau_j)$ is obtained from $g^{(1)}(\tau_j)$ through Siegert's equation (3),

$$G^{(2)}(\tau_j) = G^{(2)}_{\infty}\{1 + \beta[g^{(1)}(\tau_j)]^2\}, \quad (j = 1, \ldots, m), \quad [3]$$

where $G^{(2)}_{\infty}$ is the autocorrelation baseline and $\beta$ (<1) is an "instrumental" constant. Finally, a noisy measurement, $\tilde{G}^{(2)}(\tau_j)$, can be simulated by adding a random sequence, $\varepsilon(\tau_j)$, into Eq. [3], yielding

$$\tilde{G}^{(2)}(\tau_j) = G^{(2)}(\tau_j) + \varepsilon(\tau_j), \quad (j = 1, \ldots, m), \qquad [4a]$$

and

$$\tilde{G}^{(2)}(\tau_j) = G^{(2)}_{\infty}\{1 + \beta[\tilde{g}^{(1)}(\tau_j)]^2\}, \quad (j = 1, \ldots, m), \quad [4b]$$

where $\tilde{g}^{(1)}(\tau_j)$ is the noisy version of $g^{(1)}(\tau_j)$.

Consider now the data treatment equations. Replacing $g^{(1)}$ by $\tilde{g}^{(1)}$ in Eq. [2a] and employing vectorial notation, one obtains

$$\tilde{\mathbf{g}}^{(1)} = \mathbf{H}\hat{\mathbf{h}}, \qquad [5]$$

where $\tilde{\mathbf{g}}^{(1)}$ is a $(m \times 1)$ vector containing the normalized measurement heights, $\mathbf{H}$ is a $(m \times n)$ matrix of elements $h_{ji} = \Delta D \exp(-\Gamma_0 \tau_j / D_i)$, and $\hat{\mathbf{h}}$ is a $(n \times 1)$ vector representing the PLID estimate. Similarly, from Eqs. [1] and [2a], one can write

$$\tilde{\mathbf{g}}^{(1)} = \mathbf{F}\hat{\mathbf{f}}, \qquad [6]$$

where $\mathbf{F}$ is a $(m \times n)$ matrix of elements $f_{ji} = C_I(D_i)\Delta D \exp(-\Gamma_0 \tau_j / D_i) = C_I(D_i) h_{ji}$, and $\hat{\mathbf{f}}$ is a $(n \times 1)$ vector containing the PSD estimate. Call $\mathbf{C}$ a $(n \times n)$ diagonal matrix of components $C_I(D_i)$. Then, one can write $\mathbf{F} = \mathbf{HC}$. Substituting this last expression into Eq. [6] and comparing with Eq. [5], one finds

$$\hat{\mathbf{f}} = \mathbf{C}^{-1}\hat{\mathbf{h}}. \qquad [7]$$

In Fig. 1, the two proposed calculation paths are presented. In both methods, Eq. [4b] is first applied for obtaining $\tilde{\mathbf{g}}^{(1)}$. The "double-step method" (8, 14) first calculates a discrete PLID estimate, $\hat{\mathbf{h}}$, by numerical inversion of Eq. [5] and then uses Eq. [7] to produce the PSD estimate, $\hat{\mathbf{f}}^{\mathrm{D}}$. In the "single-step method" (15), the PSD estimate $\hat{\mathbf{f}}^{\mathrm{S}}$ is obtained in a single operation, by direct inversion of Eq. [6]. Most publications seem to adopt the double-step method. The polymer refractive index requirement and the numerical difficulties of Eq. [7] determine that most of the commercial software estimates only the PLID and $D_{\mathrm{cum}}$ instead of the PSD.

In Eqs. [5] and [6], matrices $\mathbf{H}$ and $\mathbf{F}$ must be inverted to obtain $\hat{\mathbf{h}}$ and $\hat{\mathbf{f}}$, respectively. The condition numbers of $\mathbf{H}$ and $\mathbf{F}$ (indicated by $C_{\mathbf{H}}$ and $C_{\mathbf{F}}$, respectively) measure the numerical ill conditioning of such inversions. Also, the inversion operations amplify the measurement noise, thus further deteriorating the PSD estimate. The condition number and the noise amplification are both improved by lowering the ranks of $\mathbf{H}$ or $\mathbf{F}$. However, lower ranked matrices produce PSD estimates with fewer points, and therefore a compromise is required. In general, $C_{\mathbf{H}} < C_{\mathbf{F}}$ (11), and therefore the double-step method would seem preferable. However, the propagation of errors in the second step of the double-step method (Eq. [7]) can more than compensate that condition number advantage.

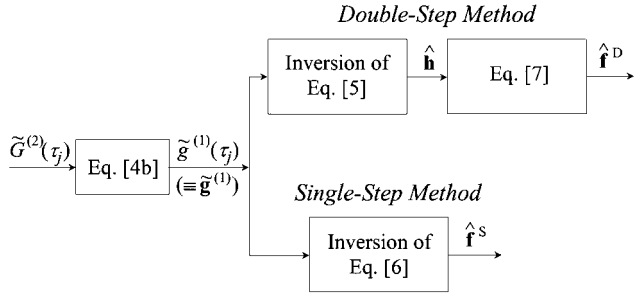


**FIG. 1.** The two calculation paths (schematic).

In a real DLS measurement, the exact PSD is unknown, and different solutions may be produced by simply readjusting the parameters of the inversion algorithm. A PSD estimate, $\hat{f}(D_i)$, may be evaluated through the following functional,

$$J_{\tilde{G}^{(2)}} = \left( \frac{\sum_{j=1}^{m} [\hat{G}^{(2)}(\tau_j) - \tilde{G}^{(2)}(\tau_j)]^2}{\sum_{j=1}^{m} [\tilde{G}^{(2)}(\tau_j)]^2} \right)^{0.5} \times 100, \quad [8]$$

where $\hat{G}^{(2)}(\tau_j) = G^{(2)}_{\infty}[1 + \beta(\sum_{i=1}^{n} f_{ji}\, \hat{f}(D_i))^2]$ is a measurement estimate. Unfortunately, the PSD estimate that minimizes Eq. [8] must be, in general, discarded due to its highly oscillatory nature, with negative peaks. Additionally, the difference between the $D_{6,5}$ estimate obtained from $\hat{f}(D_i)(\hat{D}_{6,5})$ with respect to the independently estimated $D_{\mathrm{cum}}(\hat{D}_{\mathrm{cum}})$ can be used as a practical performance index.

In contrast to real measurements, synthetic examples are ideal for evaluating alternative numerical procedures. This is because the true PSD is *a priori* specified, and therefore $\hat{f}(D_i)$ may be evaluated through, for example, the following functional:

$$J_f = \left( \frac{\sum_{i=1}^{n} [\hat{f}(D_i) - f(D_i)]^2}{\sum_{i=1}^{n} [f(D_i)]^2} \right)^{0.5} \times 100. \qquad [9]$$

## THE SIMULATED EXAMPLE

Consider the analysis of an acrylonitrile–butadiene rubber latex. Four different PSDs are proposed. Their plots are represented in Figs. 2c–2f, and their basic characteristics are given in the left-hand side of Table 1. All distributions are normal logarithmic and are defined by 41 equally spaced points in $[D_{\min}, D_{\max}]$. While $f_1$ and $f_2$ are inside the Rayleigh region,

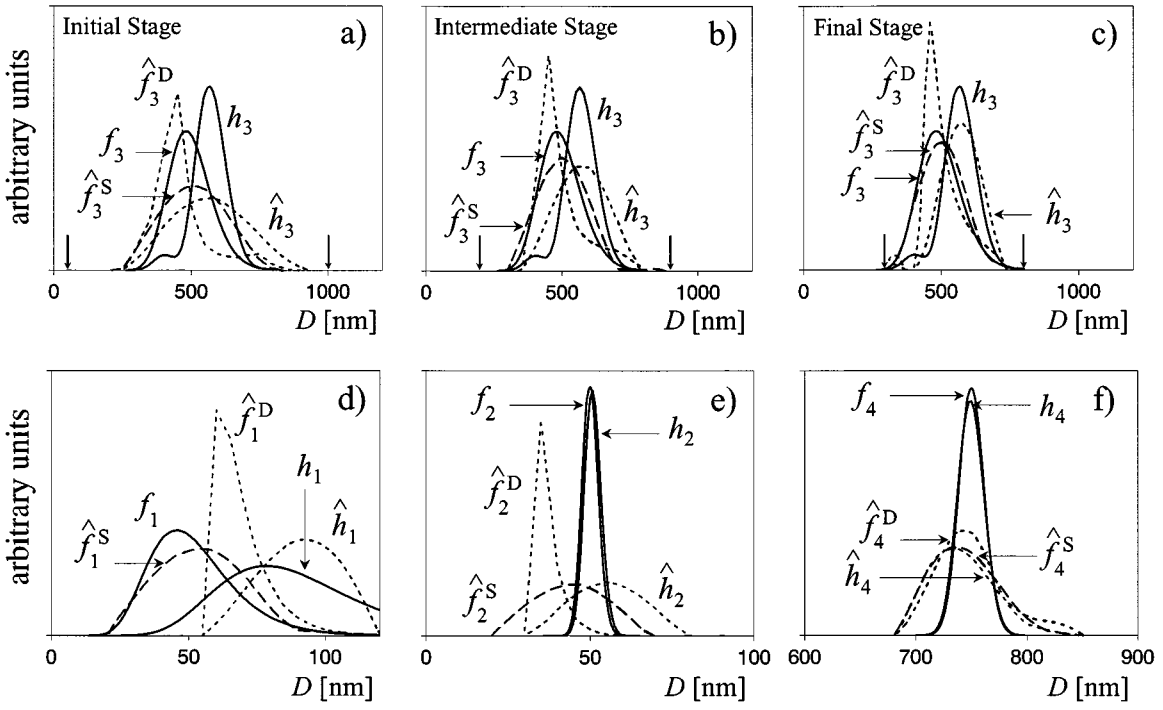


**FIG. 2.** The numerical examples. In all cases, the original PSD ( $f_i$) and the PLID ($h_i$) are compared with their corresponding estimates $\hat{f}_i$ and $\hat{h}_i$. Superscript S indicates single-step method and superscript D indicates double-step method. (a–c) Distribution $f_3$: three stages of the procedure for estimating the diameter range and the diameter interval $\Delta D$. (The adopted ranges are indicated by the vertical arrows.) (c–f) Final results for distributions $f_3$, $f_1$, $f_2$, and $f_4$.

$f_3$ and $f_4$ are outside that region. Also, $f_2$ and $f_4$ are narrow, while $f_1$ and $f_3$ are broad.

The following values are adopted for the wavelength, the detection angle, the temperature, the medium viscosity, the medium refractive index, and the polymer refractive index: $\lambda = 632.8$ nm, $\theta = 90°$, $T = 293.15$ K, $\eta = 10^{-9}$ g/(nm s), $n_m = 1.3316$ (1), and $n_p = 1.5097$ (1).

From the PSDs and $C_I(D_i)$, the PLIDs were calculated through Eq. [1] [see Figs. 2c–2f]. In a narrow diameter range, $C_I(D_i)$ varies only moderately, and for this reason, the following is approximately verified: $h_2 \propto f_2$ and $h_4 \propto f_4$. In contrast, $f_1$ and $f_3$ differ considerably from $h_1$ and $h_3$.

The function $g^{(1)}(\tau_j)$ was obtained through Eqs. [2], and the noise-free measurement $G^{(2)}(\tau_j)$ was produced through Eq. [3] with $\beta = 0.5$ and $G_\infty^{(2)} = 2 \times 10^7$. All resulting $G^{(2)}(\tau_j)$ functions vary from $3 \times 10^7$ (at $\tau_j = 0$) to $2 \times 10^7$ (at $\tau_j \to \infty$). Finally, $\tilde{G}^{(2)}(\tau_j)$ was obtained choosing $\varepsilon(\tau_j) = 10^{7/2} r(\tau_j)$ in Eq. [4a], where $r(\tau_j)$ is a random number sequence in the range $[-1, 1]$

**TABLE 1**
**Proposed PSDs and Estimation Results**

| PSD characteristics | | | | | Cumulants method | Diameter interval and diameter range | | Double-step method | | | Single-step method | | |
|---|---|---|---|---|---|---|---|---|---|---|---|---|---|
| PSD | $D_g$[a] (nm) | $\sigma$[b] | $[D_{min}, D_{max}]$ (nm) | $D_{6,5}$ (nm) | $E_{D_{cum}}$[c] (%) | $\Delta D$ (nm) | $[D_{min}, D_{max}]$[d] (nm) | $E_{D_{PSD}}$[e] (%) | $C_H$ | $J_f$ (%) | $E_{D_{PSD}}$ (%) | $C_F$ | $J_f$ (%) |
| $f_1$ | 50 | 0.300 | [0, 120] | 77.5 | 0.38 | 5 | [20, 120] | −0.85 | $7.9 \times 10^6$ | 136.8 | 0.67 | $7.1 \times 10^{15}$ | 25.5 |
| $f_2$ | 50 | 0.050 | [35, 65] | 50.7 | 0.01 | 5 | [20, 100] | −20.6 | $6.8 \times 10^6$ | 133.0 | 9.7 | $1.3 \times 10^{15}$ | 85.2 |
| $f_3$ | 500 | 0.150 | [250, 800] | 564 | −2.16 | 50 | [50, 1000] | 8.7 | $6.7 \times 10^6$ | 67.2 | 7.8 | $3.0 \times 10^{10}$ | 39.4 |
| | | | | | −2.16 | 50 | [200, 900] | 3.5 | $5.7 \times 10^6$ | 54.4 | 1.0 | $9.9 \times 10^7$ | 19.8 |
| | | | | | −2.16 | 20 | [300, 800] | −0.81 | $1.0 \times 10^7$ | 49.3 | 0.46 | $5.3 \times 10^7$ | 10.6 |
| $f_4$ | 750 | 0.015 | [700, 800] | 751 | −0.20 | 5 | [650, 850] | −0.13 | $1.6 \times 10^7$ | 59.2 | −0.17 | $2.9 \times 10^7$ | 68.4 |

[a] Geometric mean diameter.
[b] Standard deviation of $f(\ln D_i)$.
[c] $E_{D_{cum}} = (\hat{D}_{cum} - D_{6,5})/D_{6,5} \times 100$.
[d] Estimated diameter range.
[e] $E_{D_{PSD}} = (\hat{D}_{6,5} - \hat{D}_{cum})/\hat{D}_{cum} \times 100$.

with a flat probability distribution (16). Also, to allow for an adequate comparison of the different estimation results, the following was adopted: (1) in all cases, a minimal signal-to-noise ratio of around 3000 was fixed at the right-hand-side end of $\tilde{G}^{(2)}(\tau_j)$, by simply eliminating all values lower than $2.1 \times 10^7$, and (2) all $\tilde{G}^{(2)}(\tau_j)$ functions were defined by 100 evenly distributed points in their different $\tau_j$ ranges. The adopted signal-to-noise ratio is typical of a power spectrum of $\tilde{G}^{(2)}(\tau_j)$ that is observed in a good DLS measurement (e.g., after a 4 min. measurement and with a proper selection of the particle concentration). Finally, the normalized measurements $\tilde{g}^{(1)}(\tau_j)$ were obtained through Eq. [4b].

Consider now the recuperation results. First, the average diameter estimates $\hat{D}_{\text{cum}}$ were calculated employing the quadratic cumulants method (6). As expected, the relative errors in the average diameters are small (see $E_{D_{\text{cum}}}$ in Table 1).

To invert Eqs. [5] and [6], the regularization technique proposed by Twomey (13) was used. The regularization parameter (13) was selected by trial and error on the basis of (a) the observed solution, (b) the value of $J_f$, and (c) the relative error in $\hat{D}_{6,5}$ with respect to $\hat{D}_{\text{cum}}(E_{D_{\text{PSD}}})$. In general, the "best" solutions were a compromise between low $J_f$'s and small negative peaks at the distribution tails.

In both calculation methods, the following iterative procedure was applied. First, the diameter range was estimated as follows: (i) a broad enough diameter range around $\hat{D}_{\text{cum}}$ was selected, and a relatively large diameter interval between successive distribution points was sought (for example, adopting $\Delta D \approx \hat{D}_{\text{cum}}/5$); (ii) the PSDs were estimated; (iii) from the observed heights, the diameter range was reduced; and (iv) items (ii) and (iii) were repeated until the final range was found. Then, the PSD resolution was increased by reducing $\Delta D$ through a compromise between the number of distribution points and quality of results. To illustrate the proposed procedure, consider the recuperation of $f_3$. In Figs. 2a–2c and in Table 1, three stages of such recuperation are presented. Initially, a very broad diameter range was selected [Fig. 2a]. Figure 2b illustrates an intermediate stage, and Fig. 2c shows the last iteration (where the PSD is defined by 26 points).

All final results are presented in Figs. 2c–2f and in Table 1. In Figs. 2d and 2e, the distributions inside the Rayleigh region are shown. As expected, all solutions are in general poor, except perhaps for (the broader) $f_1$ via the single-step method. (Due to the propagation of errors through Eq. [7], the double-step method estimate $\hat{f}_1^{\text{D}}$ is poor, in spite of the fact that $\hat{h}_1$ is quite acceptable.) For the narrower $f_2$, the single-step method proved again to be better.

Consider the distributions outside the Rayleigh region $f_3$ and $f_4$. For (the narrower) $f_4$, both methods produce similar results. The moderate variations of $C_I(D_i)$ in a narrow diameter range determine that **F** and **H** result roughly proportional to each other, and therefore $C_{\mathbf{F}}$ and $C_{\mathbf{H}}$ are in the same order of magnitude. For an identical reason, relatively low errors are introduced in the transformation from $\hat{h}$ into $\hat{f}$, and consequently $\hat{h}_4$ and $\hat{f}_4$ are similar in shape (see Fig. 2f). For (the broader) $f_3$, the single-step method exhibits a better recuperation, in spite of the fact that $C_{\mathbf{H}} < C_{\mathbf{F}}$. As in the case of $f_1$, this happens because the condition number benefit of the double-step method is more than compensated by the errors introduced into the $h-f$ transformation [again, induced by the large variations in $C_I(D_i)$].

For completeness, the case of bimodal distributions was investigated, but no results are presented here for the sake of space. As expected, deteriorated recuperations with respect to equivalent unimodal distributions were observed. To improve the estimations, multiangle DLSs and/or a combination of single-angle DLS measurements with signals from some other optical technique ought to be employed.

## CONCLUSIONS

PSD estimates obtained from single-angle DLS measurements are in general inaccurate, due to the ill nature of the inversion operations. The problem is particularly grave for narrow distributions inside the Rayleigh region. For broader distributions inside that same region, somewhat better results are obtained, and the single-step method proved preferable.

Outside the Rayleigh region, two different situations were again observed. For narrow distributions, the shape of the PLID is close to that of the PSD estimate, and the two calculation methods produce similar results. For broad distributions, the shapes of the PLID and the PSD are quite different, and the single-step method proved again advantageous.

In summary, the relatively less-applied single-step method seems preferable to the more classical double-step method.

## REFERENCES


1. Llosent, M. A., Gugliotta, L. M., and Meira, G. R., *Rubber Chem. Technol.* **69,** 696 (1996).
2. Barth, H. G., and Sun, S. T., *Anal. Chem.* **57,** 151R (1985).
3. Pecora, R., "Dynamic Light Scattering. Applications of Photon Correlation Spectroscopy." Plenum Press, New York, 1985.
4. Kourti, T., and MacGregor, J. F., *in* "Particle Size Distribution II. Assessment and Characterization" (T. Provder, Ed.), ACS Symposium Series 472, Chap. 3. American Chemical Society, Washington, DC, 1991.
5. Thomas, J., *J. Colloid Interface Sci.* **117,** 187 (1987).
6. Koppel, D. E., *J. Chem. Phys.* **57,** 4814 (1972).
7. Mie, G., *Ann. Phys.* **25,** 337 (1908).
8. Stock, R., and Ray, W., *J. Polym. Sci. Polym. Phys. Ed.* **23,** 1393 (1985).
9. Provencher, S. W., *Comput. Phys. Commun.* **27,** 213 (1982).
10. Finsy, R., *Adv. Colloid Interface Sci.* **52,** 79 (1994).
11. De Vos, C., Deriemaeker, L., and Finsy, R., *Langmuir* **12,** 2630 (1996).
12. Bryant, G., and Thomas, J., *Langmuir* **11,** 2480 (1995).
13. Twomey, S., *Franklin. Inst.* **279,** 95 (1965).
14. Bott, S. E., *in* "Particle Size Distribution. Assessment and Characterization" (T. Provder, Ed.), ACS Symposium Series 332, Chap. 5, p. 74. American Chemical Society, Washington, DC, 1987.
15. Stock, R., and Ray, W., *in* "Particle Size Distribution. Assessment and Characterization" (T. Provder, Ed.), ACS Symposium Series 332, Chap. 7, p. 105. American Chemical Society, Washington, DC, 1987.
16. Gulari, E., Tsunashima, Y., and Chu, B., *J. Chem. Phys.* **70,** (1979).